Onset of axisymmetric sloshing in a food processor

Tomoaki Watamura* and Kazuyasu Sugiyama
Graduate School of Engineering Science, Osaka University, 1-3, Machikaneyama, Toyonaka, Osaka 560-8531, Japan

(Received 2 September 2021; revised 15 November 2021; accepted 17 November 2021; published 8 December 2021)

We report on the axisymmetric oscillation at the air-water interface in a food processor and Taylor-Couette systems. To gain insights into the mechanisms of free-surface oscillation, we conduct a series of experiments on the visual observations of free-surface deformation and the velocity measurements. At relatively low rotation speeds, the surface height at the rotating object surface decreases but remains stationary. As the rotation speed increases in small increments, oscillation begins when the deformed free surface detaches from the rotating object, and its onset depends strongly on the initial surface height. To account for the similarity mechanism of the onset, a scaled surface deformation based on the bulk Froude number is introduced herein; we find that the oscillation occurs at the scaled surface deformation beyond unity. These findings explain the causal relationship between the surface deformation and the oscillation onset and help to predict its occurrence to avoid mechanical damage to an apparatus with rotating components.

DOI: 10.1103/PhysRevE.104.065104

I. INTRODUCTION

The free surface in a rotating system exhibits drastic deformation. This phenomenon has motivated studies on fluid motion in the contexts of nature (e.g., bathtub vortex [1]) and engineering (e.g., hydraulic or turbomachinery [2,3]). Even in a cylindrical container, which can be considered as the simplest system, we can find a variety of interface shapes and their motions can be observed depending on the container size, fluid volume, density or viscosity ratio, external forcing, etc. Thus, the interface shape between two fluids has been studied extensively: for instance, two immiscible liquids or gas-liquid two-phase flows in a cylindrical container [4–10] and in concentric double cylinders (termed as the Taylor-Couette system) [11,12]. In these configurations, at relatively high rotation speeds, the surface deformations become unstable and exhibit time-dependent behaviors owing to azimuthal instability [6–8]. On a kitchen table, we can also observe an air-water interface deformation in a food processor, which comprises rotating blades and a cylindrical container; in this case, oscillations in surface elevation often occur after just a few seconds of blending.

In a stationary cylindrical container including a rotating bottom plate, a swirling wave with an azimuthal wave number $m \neq 0$ is excited by flow-induced instabilities [6,7]. Under external forcing, in an upright cylindrical container [10,13] or an annular tank [14], a nonaxisymmetric wave is also imposed on the surface deformation; this is called "sloshing." Axisymmetric ($m = 0$) sloshing in a rotating system, such as the periodic oscillation of surface elevation in a food processor and turbomachinery [3], is a frequently observed phenomenon; however, because the flow is quite turbulent and includes numerous bubbles, the mechanism of oscillation remains unclear. These unsteady motions of the free surface obstruct mixing and cause mechanical damage; thus, for safe operation, it is necessary to predict its onset prior to use. As a possible mechanism of the sloshing, usually involving complex phenomena of free boundary turbulence, the stabilities of azimuthal shear [6,7] or swirling flows [15] may cause the sudden transition to sloshing motion. However, a detailed and accepted explanation of the oscillation onset is lacking. To shed more light on the issue, we perform systematic experiments for clarifying the onset condition of axisymmetric sloshing in a cylindrical container including a high-speed rotating object. Visual observations of the flow in a food processor and Taylor-Couette systems reveal that the oscillation begins when the deformed free surface detaches from the rotating object. We propose a transition model with a scaled surface deformation based on the bulk Froude number and discuss the mechanism of the oscillation onset.

II. EXPERIMENT

We study the gas-liquid interface motion in three different apparatuses: a food processor (FP; Tiger Company, SKT-N100K), and two Taylor-Couette (TC) systems; the two TC systems are referred to as TC1 and TC2. Figure 1 outlines the experimental setups and coordinate systems. The containers with radius R_o are made of transparent plastics to allow visualization. In the FP, the six-piece blade with tip radius R_i is driven by an electric motor; its rotation speed Ω is adjusted in the range of 1800 rpm $\leqslant \Omega \leqslant$ 6600 rpm using a voltage controller. In the TC systems, the top and bottom end plates are stationary, and the inner cylinders with radius R_i are made of stainless steel and are driven by a speed control motor via a torque meter; its rotation speed Ω ranges in 1000 rpm $\leqslant \Omega \leqslant$ 5000 rpm, and is set at every 100 rpm. In each run of TC1, the rotation speed Ω is initially incremented from 1000 to 5000 rpm, and then is decremented from 5000

*tomoaki.watamura@me.es.osaka-u.ac.jp

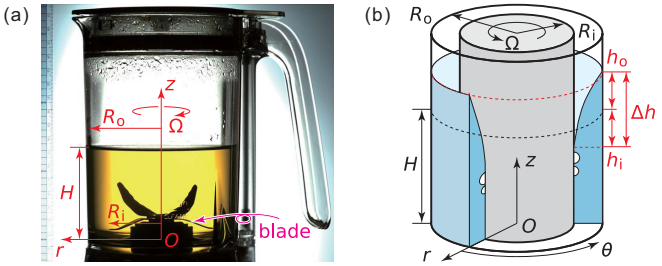

FIG. 1. Experimental configurations of the (a) food processor (FP) and (b) Taylor-Couette (TC) system. In (a), the outer cylinder with radius $R_o = 50$ mm is stationary and the blade with radius $R_i = 30$ mm rotates at rotation speed Ω. The container height is 140 mm. In (b), the outer cylinders with radius $R_o = 37.5$ mm for TC1 and $R_o = 75$ mm for TC2 are stationary. The inner cylinders with radius $R_i = 25$ mm for TC1 and $R_i = 50$ mm for TC2 rotate at Ω. The container heights are 700 mm for TC1 and 1000 mm for TC2. In these systems, the containers are first partially filled with tap water up to height H.

to 1000 rpm. When the rotation speed is changed, we let the system settle for a few minutes, in order to ensure the decay of the transient motion such as an irregular oscillation and an azimuthal wave $m \neq 0$. The containers are partially filled with tap water at a temperature of $24 \pm 1\,^{\circ}$C, dynamic viscosity of $\mu = 0.9\times10^{-3}$ Pa s, and a density of 997 kg/m^3. Different quiescent water levels H are studied.

The shape of the free surface is visualized by backlighting with an LED light. Colored dye is added to the tap water to obtain a clear interface profile. The interface motion is captured using a high-speed video camera. Particle image velocimetry (PIV) is employed to measure the azimuthal velocity distribution. The laser-induced fluorescence (LIF) technique is applied to PIV [17] to distinguish tracer particles within the bubbly flow. Fluorescent tracer particles with a diameter of 15 μm were seeded at 0.03 vol % into the water. The laser light reflected from the particle interface is blocked by an optical long-pass filter, with most of the remainder of the fluorescent light passing through the filter. To measure the velocity profile along the z axis, a high-speed video camera and laser optics are mounted on a traverse stage and vertically traverse for ∼350 mm. The camera is placed at an angle of ∼40° to measure the velocity profile along the r axis. For precise velocity measurements, we use a calibration plate, on which 2 mm × 4 lattices with 0.2-mm-wide white lines are made by machining. Using the position of the crossing of the lines, 5×9 sectors are transformed into the r-θ (Cartesian) positions. The maximum error due to image distortion is approximately 2% in space. On the basis of guide to expression of uncertainty in measurement ISO [18], we estimate the uncertainty in the azimuthal velocity measurement at 95% confidence to be 6% relative to the wall velocity.

III. RESULTS AND DISCUSSION

We observe the gas-liquid interface shape in the FP and find remarkable changes in the fluid motion, as shown in Fig. 2. As the blades are set into rotation, the centrifugal force pushes the fluid outward, and thus the free surface deforms [see Fig. 2(a) and movies are available in the Supplemental Material [16]]. At a relatively low Ω (e.g., Ω = 2400 rpm), although small bubbles disperse in the bulk fluid, the interface shape is as a paraboloid of revolution [Fig. 2(a)] and remains stationary [Fig. 2(b)], similar to that on a rotating disk [7]. When the rotation speed Ω is sufficiently high, the interface becomes spontaneously unstable, and its axisymmetric periodic deformation, i.e., sloshing, commences [Fig. 2(c)]. As observed from the top of the apparatus, we find that the free surface intermittently detaches from the rotating blades when sloshing occurs. The course of this periodic phenomenon can be qualitatively understood as follows: The centrifugal force pushes the liquid toward the outer wall; the free surface detaches from the rotating blades; the viscous and turbulent

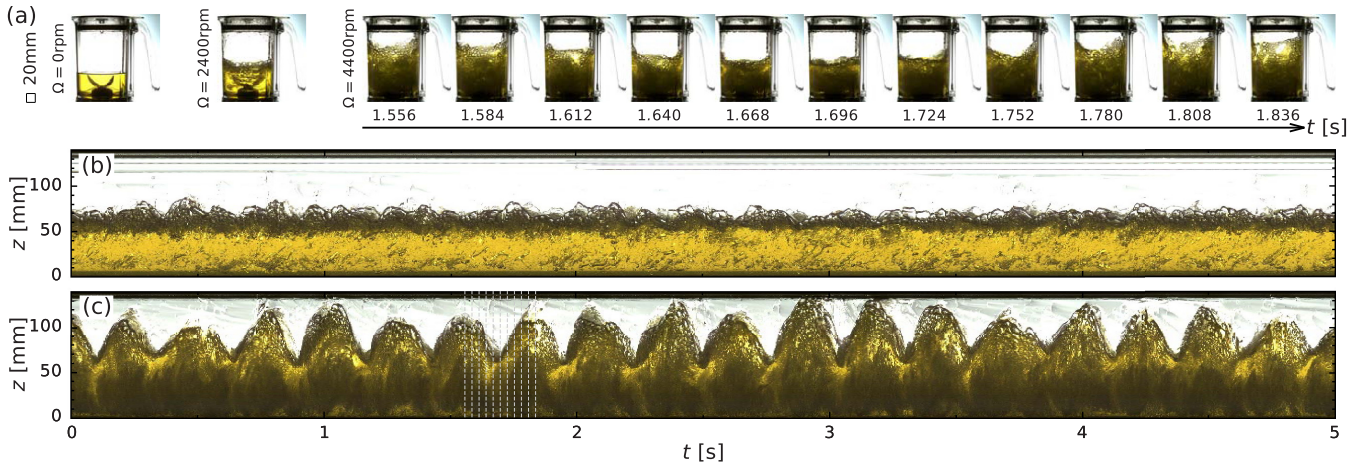

FIG. 2. Flow pattern in the FP. (a) Snapshots for different rotation speeds Ω. The container is partially filled with tap water to $H = 50$ mm. Surface deformation is stationary at Ω = 2400 rpm and becomes time dependent at Ω = 4400 rpm; the time interval between frames is 28 ms, corresponding to 1/10 of one oscillation period. The temporally expanded image of the free surface extracted near the outer cylinder wall ($r = R_i + 3/4d$) at (b) Ω = 2400 rpm and (c) Ω = 4400 rpm. In (c), the vertical white dotted lines correspond to the sequential instants in (a). The darker region includes bubbles because bubbles block backlighting. The corresponding movie is available in the Supplemental Material [16].

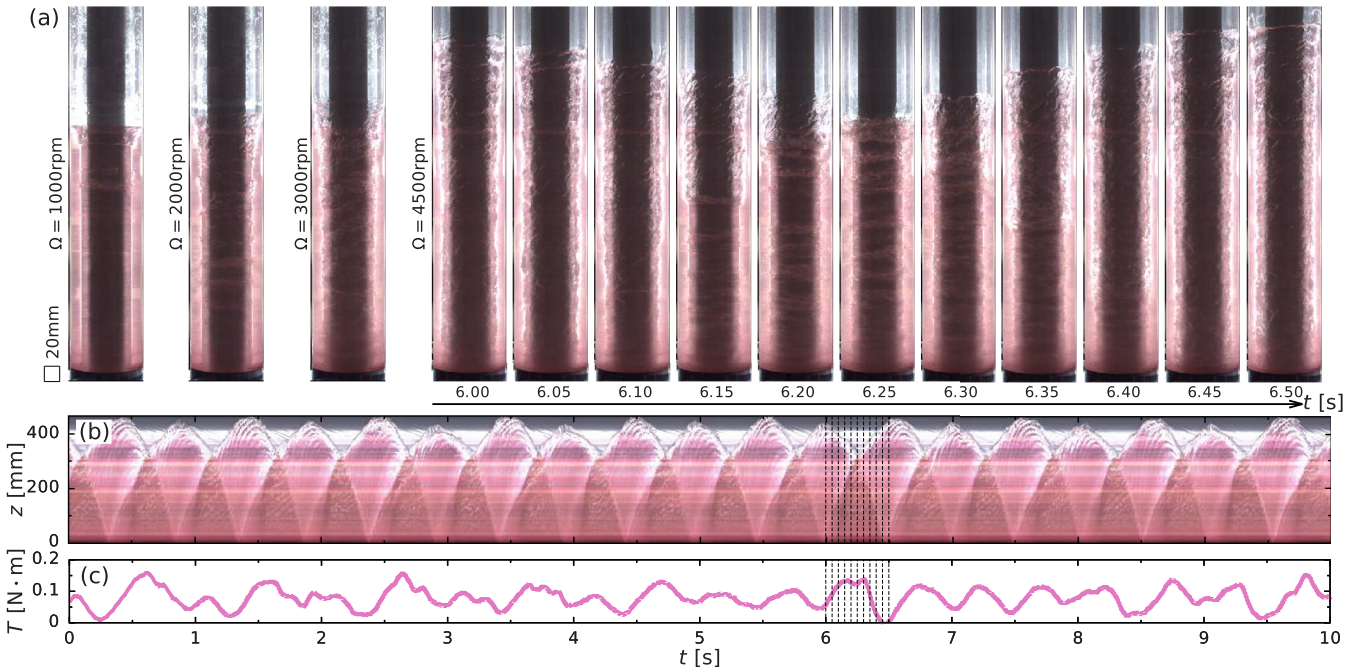

FIG. 3. Flow pattern in the TC system (TC1) comprising the inner cylinder with radius $R_i = 25$ mm and the outer cylinder with radius $R_o = 37.5$ mm. (a) Snapshots for different rotation speeds Ω. The inner cylinder is partially filled with tap water to $H = 300$ mm. Surface deformation is stationary at $\Omega < 3000$ rpm and becomes time dependent at $\Omega = 4500$ rpm; the time interval between frames is 50 ms, corresponding to 1/10 of one oscillation period. (b) Temporally expanded image of the free surface extracted near the outer cylinder wall ($r = R_i + 3/4d$) at (b) $\Omega = 4500$ rpm. The lighter region forms near the gas-liquid interface, which scatters the backlight. (c) Temporal variation of the torque acting on the inner cylinder. The torque is measured simultaneously with the flow visualization corresponding to (b). The vertical black dotted lines in (b) and (c) correspond to the sequential instants in (a). The corresponding movie is available in the Supplemental Material [16].

dissipations reduce the swirling liquid speed; the effect of gravity flattens the free surface, likely to recover to a stationary one; and finally, the rotating object drives the liquid again. Note that we measure the oscillation amplitude for various numbers of blades and infer that the sloshing behavior depends on the number of blades (details are in Appendix A). It is difficult to precisely determine when the free surface detaches from the rotating blades owing to the entrained bubbles and the complexity of the blade shape. For these reasons, we are unable to obtain quantitative evidence to suggest a clear causal relationship between the surface deformation and the sloshing motion in FP.

To overcome these difficulties, we again observe the interface deformation but in a TC system as a simpler axisymmetric system. As the rotation speed Ω increases, the surface deformation increases, and a sudden transition to sloshing motion occurs [see Fig. 3(a) and movies are available in the Supplemental Material [16]]. Figure 3(b) shows the temporal variation in the fluid distribution near the outer cylinder and indicates periodic surface deformation, similar to that in the FP [Fig. 2(c)]. The torque acting on the inner cylinder [Fig. 3(c)], which is simultaneously measured with the flow visualization, exhibits temporal fluctuation and is negatively correlated with the surface elevation, indicating a Pearson correlation coefficient of -0.40 [see Fig. 7(a) and Appendix B]: The torque decreases when the liquid is pushed toward the outer wall, whereas it increases when the surface is flattened.

To estimate the centrifugal force, we measure the azimuthal velocity via PIV-LIF on a vertical traverse stage which enables us to precisely locate the optics system along the z axis [Fig. 4(a)]. The captured images are calibrated into the r-θ coordinates [Fig. 4(b)]. To validate the measurement accuracy, we compare the axially averaged azimuthal velocity profile $\langle \overline{u}_\theta \rangle_z$ for a single phase flow (i.e., the inner cylinder is fully immersed) with the Reynolds number $\mathrm{Re}(\equiv \rho U d/\mu) = 1\times10^5$ using PTV [19], where $\overline{\cdots}$ denotes the time average, $\langle \cdots \rangle_z$ denotes the axial average, $U \equiv \Omega R_i$ is the wall velocity, and $d \equiv R_o - R_i$ is the gap clearance. Our PIV data are found to be completely consistent with PTV, even though there exists a difference originating from the radius ratio [20]; the bulk velocity decreases with decreasing the radius ratio $\eta \equiv R_i/R_o$ ($\eta = 0.667$ for the present and $\eta = 0.716$ for Ref. [19]). We measure the velocity profile for different Ω at $H = 300$ mm and find that the normalized velocity $\langle \overline{u}_\theta \rangle_z / U$ decreases with increasing Ω, in which case the deformation of the free surface [see the insets of Fig. 4(c)] and the entrainment of bubbles (see also the Supplemental Material [16]) suppress the momentum transfer from the inner cylinder. The secondary flows (u_r and u_z) and their structure, i.e., Taylor vortex, may affect the free-surface profile, and vice versa. Thus, a detailed measurement is a key subject for further studies on surface deformation. This study primarily focuses on the onset of sloshing; for this reason, the details regarding the secondary vortical structure will be investigated in a future work.

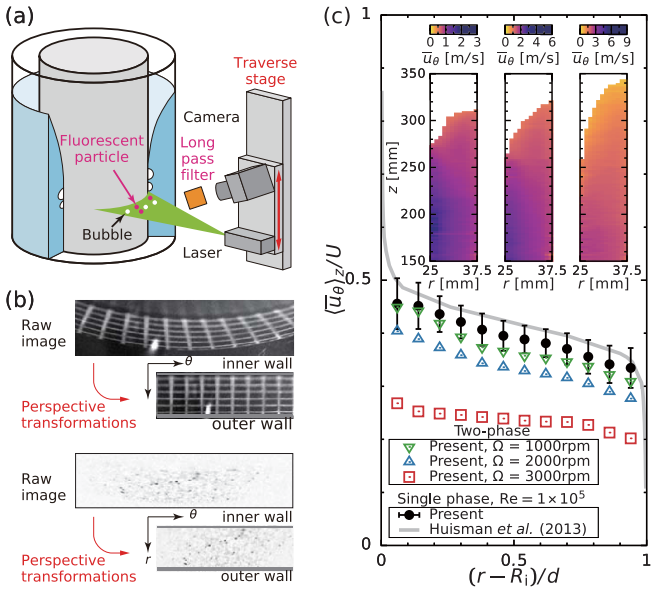

FIG. 4. Measurement of the azimuthal velocity profile in the TC system (TC1). (a) Experimental setup for PIV applying LIF: A high-speed video camera and laser optics are mounted on a vertical traverse stage. To measure the velocity profile along the radial direction, a laser sheet is placed horizontally, and a high-speed camera is placed at a tilt angle of ∼40°. (b) Imaging calibration: Images are transformed into the r-θ coordinates via perspective transformations (top). Azimuthal velocity profile along the radial direction is measured by PIV using a particle image in the r-θ coordinates (bottom). (c) Temporally and axially averaged azimuthal velocity profile: The insets show time-averaged azimuthal velocities on the r-z cross section for various rotation speeds Ω (from left to right, Ω = 1000 rpm, Ω = 2000 rpm, and Ω = 3000 rpm). Error bars show the standard deviation of the temporal variation.

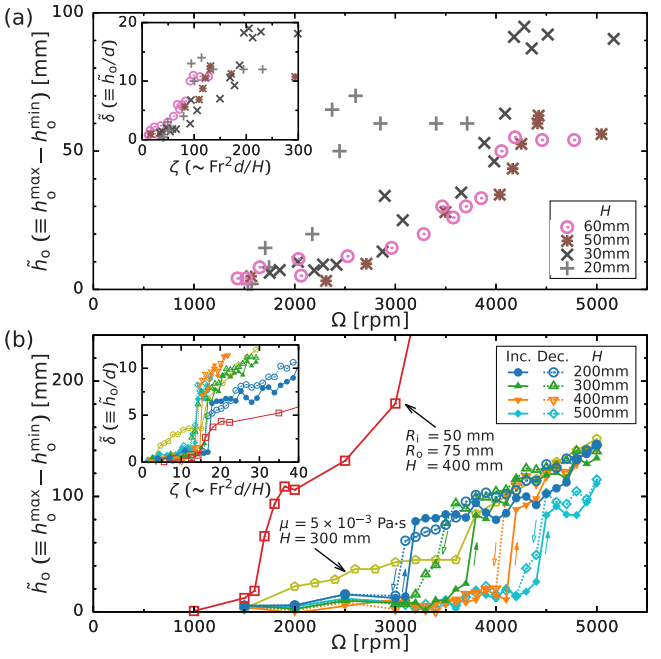

FIG. 5. Oscillation amplitude of surface deformation at the outer wall in the (a) FP and (b) TC systems. In (a), the oscillation amplitudes exhibit plateaus at high Ω because the free surface reaches the FP lid. In (b), blue, green, orange, cyan, and yellow symbols refer to the measurements for TC1, whereas the red symbols refer to measurements for TC2. Clear hysteresis exists between the increasing and decreasing ramps. Insets show the bifurcation diagram of the normalized oscillation amplitude $\tilde{\delta} \equiv \tilde{h}_o/d$ vs the scaled surface deformation $\zeta \sim \mathrm{Fr}^2\, d/H$.

Next, we plot the oscillation amplitude of the surface deformation at the outer cylinder $\tilde{h}_o (\equiv h_o^{max} - h_o^{min})$ with respect to the rotation speed Ω, as shown in Fig. 5. The oscillation commences at Ω ≈ 2000 rpm in the FP. For $H \geqslant 60$ mm, an azimuthal wave $m = 2$ is imposed on the free surface. Such flows are prone to symmetry breaking because of the degree of freedom of the flow [8]. Therefore, the oscillation amplitude $\tilde{h}_o$ at $H = 60$ mm is slightly larger than that at the other H. An azimuthal wave $m = 1, 2$ intermittently appears at $H = 50$ mm and Ω > 5000 rpm; in this case, the oscillation amplitude decreases with the number of blades [see Fig. 6(b) and Appendix A]. Traveling wave motions that differ from the axisymmetric sloshing are no longer able to be eliminated. Nevertheless, the onset of sloshing is insensitive to the number of blades. In the case of TC1, the onset of sloshing ranges 3000 rpm < Ω < 4500 rpm and exhibits a clear hysteresis when increasing or decreasing the ramp of Ω. Background turbulence may cause a flow transition in the surface motion; such hysteresis can be also observed in rotating flow systems [7,12].

Here, to address the similarity mechanism of the oscillation onset, we shall consider the stationary shape of the interface determined by the interplay between the gravitational and centrifugal forces. Supposing the pressure on the free surface to be constant, we can describe the surface profile as $\partial h/\partial r = \overline{u}_\theta^2/(rg)$. At the inner wall surface ($r = R_i$), we obtain $\partial h/\partial r = \mathrm{Fr}^2$, which yields the surface deformation $\Delta h (\equiv h_o - h_i) \sim \int_{R_i}^{R_o} \mathrm{Fr}^2\, \mathrm{d}r = \mathrm{Fr}^2\, d$, where $\mathrm{Fr} \equiv U(R_i g)^{-1/2}$ is the surface Froude number based on the wall velocity. Visual observations indicate that axisymmetric sloshing begins when the free surface detaches from the rotating object. Accordingly, we hypothesize that the oscillation occurs beyond a critical value of the scaled surface deformation $\zeta (\equiv \Delta h/H) \sim \mathrm{Fr}^2\, dH^{-1}$ as a result of the insulation of the liquid momentum transfer from the rotating object due to the surface detachment therefrom. Determined from a jump in the profile of the scaled oscillation amplitude $\tilde{\delta} \equiv \tilde{h}_o/d$ vs ζ, the flow transition is arranged to occur at $\zeta \approx 15$ in TC flows [see the inset of Fig. 5(b)], where the corresponding Reynolds number reaches $\mathrm{Re} > 1\times10^5$. Despite the complexity in the blade shape and the velocity profile in the FP, the flow transition can be also determined at $\mathrm{Fr}^2\, dH^{-1} \sim O(10)$, as shown in the inset of Fig. 5(a). Here, as shown in Fig. 4(c), the bulk azimuthal velocity in the TC flow decreases to $\langle \overline{u}_\theta \rangle_{rz}/U \approx 1/4$, where $\langle \cdots \rangle_{rz}$ denotes the radial and axial averages. Therefore, based on the bulk azimuthal velocity $\langle \overline{u}_\theta \rangle_{rz}$, we obtain the bulk Froude number $\mathrm{Fr}^* \approx U(R_i g)^{-1/2}/4$ and rescale the scaled surface deformation $\zeta^* \sim \mathrm{Fr}^{*2}\, dH^{-1} \approx \mathrm{Fr}^2\, dH^{-1}/16$. An interesting result of this scaling analysis is that the flow transition occurs at $\zeta^* \approx 1$, indicating that the oscillation onset is in excellent accord with a qualitative understanding of

the dynamics involving surface detachment from the rotating object. Here, we also measure the sloshing period. Over a wide range of the scaled surface deformation ζ, the sloshing period is found to be in good agreement with that from the linearized model [3]. Therefore, we conclude that the sloshing motion is analogous to an oscillating liquid column (details are in Appendix B).

Finally, we perform additional experiments. (i) For a larger apparatus (TC2) with an initial surface height $H = 400$ mm, we determine the onset of the transition in TC2 at $\mathrm{Fr}^2\, dH^{-1} \approx 15$ and $\mathrm{Re} \approx 2\times10^5$ [see Fig. 5(b)]. (ii) In the same system (TC1) but with the addition of the surfactant (Triton X-100) or with a hydrophobic/hydrophilic paint coating on the surface of cylinders, we observe that the oscillation onset is significantly modified by the addition of the surfactant and weakly depends on the contact angle (details are in Appendix C). (iii) In the same system (TC1) but with increasing dynamic viscosity $\mu \approx 5\times10^{-3}$ Pa s, using a glycerol aqueous solution, we observe a rapid increase in the oscillation amplitude at $\mathrm{Fr}^2\, dH^{-1} \approx 15$ and $\mathrm{Re} \approx 2\times10^4$; however, the amplitude gradually increases below the critical point [see Fig. 5(b)]. These experimental results indicate the crucial importance of the turbulent flow structure: Turbulent Taylor vortices, i.e., vertically aligned coherent torus structures, persist up to $\mathrm{Re} < 4\times10^4$; for larger Re, the flow becomes irregular and turbulent, and distinct Taylor vortices are not directly visible [21–24]. We can thus conclude that the nonuniformity of the turbulence owing to the presence of Taylor vortices triggers the oscillation of the free surface below the critical point.

IV. CONCLUSION

The axisymmetric oscillating motions of the gas-liquid interface in a food processor and two Taylor-Couette systems were experimentally studied. Visual observations of the surface shape helped classify the flow mode as stable deformation and axisymmetric sloshing (periodic axisymmetric surface elevation). In Taylor-Couette systems, the bifurcation diagram constructed by the amplitude of surface oscillation as a scaled surface deformation based on the bulk Froude number shows that the amplitude increases rapidly at the critical point. We found that the transition occurs at unity of the scaled surface deformation ζ^*. Note that since the expression of ζ^* includes no material property, only the system kinematics and geometry would determine the transition. Therefore, the surface oscillation mechanism can be understood as the following processes: The centrifugal force pushes the liquid toward the outer wall; the free surface detaches from the inner cylinders; the viscous and turbulent dissipations reduce the swirling liquid speed; the effect of gravity flattens the free surface; and finally, the liquid is driven again. We found that the same transition occurs in a food processor, even though it is indistinct; the surface detachment from the rotating object is a key factor in the mechanism of axisymmetric surface sloshing.

Some remarkable features were also noted: the generation of an azimuthal wave and the excitation below the critical point. These flows exhibit more complex behaviors owing to the turbulent vortex structure; thus, they show a potential for application in the mixing of density-stratified fluids such as oil-water mixtures or particle suspensions. As the size and rotation speed evaluated here fall within the range of industrial applications, such as pumps or mixing facilities, this study lays the foundation for predicting violent sloshing in turbomachineries as well as in food processors.

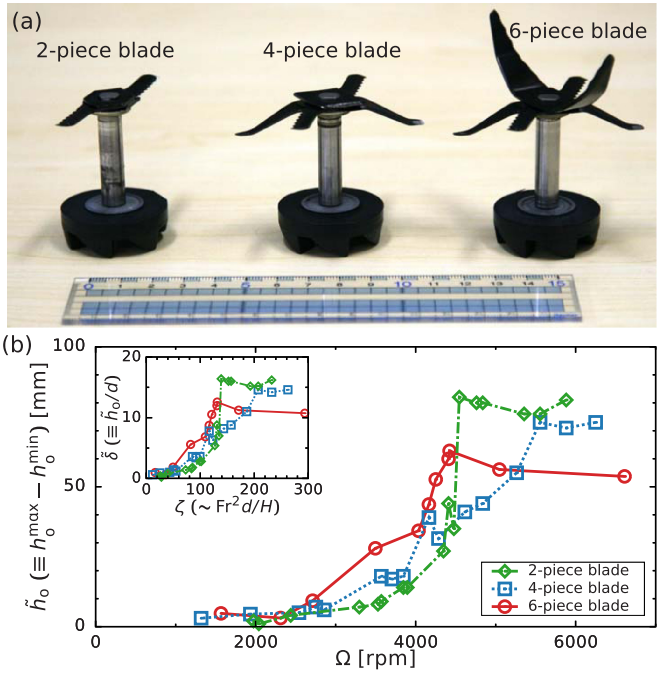

FIG. 6. (a) A snapshot of mixing blades. (b) Oscillation amplitude of surface deformation in the FP for different number of blades.

ACKNOWLEDGMENTS

We acknowledge Professor Dr. Y. Tsujimoto, Professor Emeritus of Osaka University, and Dr. K. Yonezawa, Central Research Institute of Electric Power Industry, for giving us essential information and for fruitful discussions.

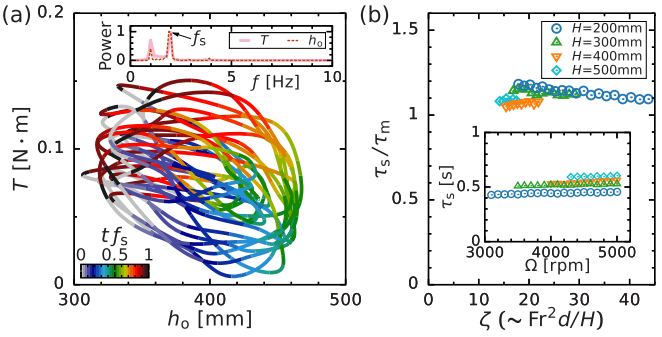

FIG. 7. (a) Lissajous plot of the torque T and the surface elevation h_o. The inset shows the power spectra of T and h_o. Color indicates the scaled time tf_s, where f_s is the sloshing frequency determined as a peak frequency in a power spectrum. (b) The scaled sloshing period τ_s/τ_m vs the scaled surface deformation ζ. The inset shows the effect of the rotation speed Ω on the measured sloshing period τ_s.

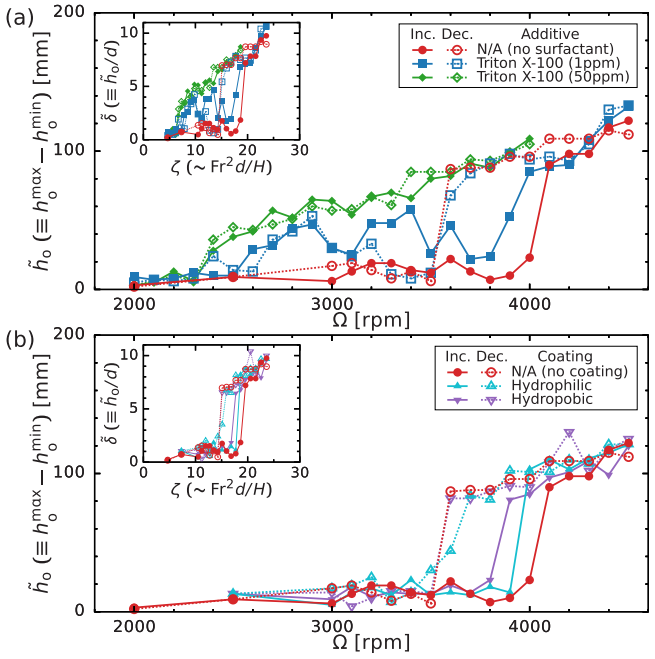

FIG. 8. Oscillation amplitude of surface deformation at $H =$ 300 mm for different (a) concentrations of the surfactant Triton X-100 and (b) contact angles of the surface of the cylinders.

APPENDIX A: EFFECT OF THE NUMBER OF MIXING BLADES

To test the effect of the number of blades on the sloshing motion in FP, from the six-piece blade, we cut blades off from the shaft using a hacksaw and prepare two- and four-piece blades [see Fig. 6(a)]. We visually observed the amplitude of sloshing driven by the two/four/six-piece blades in the FP, as shown in Fig. 6(b). For $\Omega < 4000$ rpm, the oscillation amplitude $\tilde{h}_o$ increases with the number of blades, which determines the driving force. On the other hand, for $\Omega > 5000$ rpm, the oscillation amplitude decreases with the number of blades. In this region, an azimuthal wave $m = 1, 2$ intermittently appears, and we infer that a rotating object with a non-azimuthal-symmetric shape excites an azimuthal instability. The details of the azimuthal wave will be investigated in a future work.

APPENDIX B: TEMPORAL CHARACTERISTICS OF SLOSHING

To visualize the relationship between the torque and the free-surface elevation near the outer cylinder, we plot the temporal variation as a Lissajous orbit, as shown in Fig. 7(a). We note a negative correlation with the Pearson correlation coefficient of $\mathrm{cov}(T, h_o)/[\sigma(T)\sigma(h_o)] = -0.40$, where cov is the covariance and σ is the standard deviation. Figure 7(b) shows the scaled sloshing period τ_s/τ_m with respect to the scaled surface deformation ζ, where τ_s is the experimentally measured sloshing period $\tau_s(\equiv 1/f_s)$ and $\tau_m\{\approx \pi[(h_o^{max} + H)/g]^{1/2}\}$ is the timescale employed in the linearized sloshing model [3]. We find that the scaled sloshing period ranges at unity, indicating that this sloshing motion is analogous to an oscillating liquid column.

TABLE I. Contact angle of water droplet [mean $\pm$ SD (deg)].

Coating	Inner cylinder	Outer cylinder
N/A (no coating)	93 ± 6	73 ± 5
Hydrophobic	95 ± 6	95 ± 2
Hydrophilic	52 ± 6	22 ± 4

APPENDIX C: EFFECT OF SURFACTANT AND CONTACT ANGLE

To test the effect of surface tension on the sloshing motion in a TC system, the surface tension is lowered by adding surfactant (Triton X-100). The surface tension between water and air is known to be 73 mN/m. After the addition of 1 or 50 ppm of Triton X-100, the surface tension decreases to 60 or 32 mN/m [25]. Furthermore, the addition of the surfactant prevents bubble coalescence due to a nonuniform contamination distribution along the bubble surface, known as the Marangoni effect [26]; therefore, small bubbles, which are formed in strongly turbulent shear flow, distribute over the entire of liquid between the cylinders, and the bubbly liquid becomes very opaque. Such a bubble suspension behaves as a non-Newtonian liquid [27,28], leading to modifications of turbulence and momentum transfer [29–31]. Due to this complex nature of bubbly liquids, it is difficult to justify the contributions of the surface tension and the Marangoni effect, and therefore we observe the effect of surfactant on the onset of sloshing hereafter. As shown in Fig. 8(a), by adding minute concentrations (1 ppm) of the surfactant, we observe a disordered increase of the sloshing amplitude. By adding a high concentration (50 ppm) of the surfactant, the rapid increase in the sloshing amplitude no longer appears. These results indicate that the addition of surfactant significantly affects the onset of sloshing, and suggest that modifications of the effective viscosity and turbulent flow structure are reflected in the onset [cf. the dynamic viscosity dependency of the transition shown in Fig. 5(b)].

We also perform experiments with different contact angles. Both the inner and outer cylinders are coated with hydrophobic or hydrophilic paint, and the resulting contact angles are measured using the half-angle method; the results are summarized in Table I. Figure 8(b) shows the transition of the oscillation amplitude for different contact angles and indicates that the contact angle has only a minor effect on the onset of oscillation.

[1] A. H. Shapiro, Bath-tub vortex, Nature (London) **196**, 1080 (1962).

[2] S. Mulligan, G. De Cesare, J. Casserly, and R. Sherlock, Understanding turbulent free-surface vortex flows using a Taylor-Couette flow analogy, Sci. Rep. **8**, 824 (2018).

[3] K. Yonezawa, K. Nishimura, T. Sano, K. Miyagawa, and Y. Tsujimoto, Sloshing of fluid between rotating inner vertical

shaft and stationary outer casing, J. Fluid Eng. **143**, 121108 (2021).

[4] T. G. Lim, S. Choi, and J. M. Hyun, Transient interface shape of a two-layer liquid in an abruptly rotating cylinder, J. Fluid Eng. **115**, 324 (1993).

[5] K. Y. Kim and J. M. Hyun, Spin-up from rest of a two-layer liquid in a cylinder, J. Fluid Eng. **116**, 808 (1994).

[6] T. R. N. Jansson, M. P. Haspang, K. H. Jensen, P. Hersen, and T. Bohr, Polygons on a Rotating Fluid Surface, Phys. Rev. Lett. **96**, 174502 (2006).

[7] Y. Tasaka and M. Iima, Flow transitions in the surface switching of rotating fluid, J. Fluid Mech. **636**, 475 (2009).

[8] S. Fujimoto and Y. Takeda, Topology changes of the interface between two immiscible liquid layers by a rotating lid, Phys. Rev. E **80**, 015304(R) (2009).

[9] P. T. Brady, M. Herrmann, and J. M. Lopez, Two-fluid confined flow in a cylinder driven by a rotating end wall, Phys. Rev. E **85**, 016308 (2012).

[10] M. Reclari, M. Dreyer, S. Tissot, D. Obreschkow, F. M. Wurm, and M. Farhat, Surface wave dynamics in orbital shaken cylindrical containers, Phys. Fluids **26**, 052104 (2014).

[11] D. Bonn, M. Kobylko, S. Bohn, J. Meunier, A. Morozov, and W. van Saarloos, Rod-Climbing Effect in Newtonian Fluids, Phys. Rev. Lett. **93**, 214503 (2004).

[12] N. Mujica and D. P. Lathrop, Hysteretic gravity-wave bifurcation in a highly turbulent swirling flow, J. Fluid Mech. **551**, 49 (2006).

[13] P. A. Caron, M. A. Cruchaga, and A. E. Larreteguy, Study of 3D sloshing in a vertical cylindrical tank, Phys. Fluids **30**, 082112 (2018).

[14] O. M. Faltinsen, I. A. Lukovsky, and A. N. Timokha, Resonant sloshing in an upright annular tank, J. Fluid Mech. **804**, 608 (2016).

[15] V. Shtern and F. Hussain, Collapse, symmetry breaking, and hysteresis in swirling flows, Annu. Rev. Fluid Mech. **31**, 537 (1999).

[16] See Supplemental Material at http://link.aps.org/supplemental/10.1103/PhysRevE.104.065104 for videos of the sloshing motion in FP and TC1.

[17] R. Lindken and W. Merzkirch, A novel PIV technique for measurements in multiphase flows and its application to two-phase bubbly flows, Exp. Fluids **33**, 814 (2002).

[18] ISO, *Guide to the Expression of Uncertainty in Measurement* (ISO, Geneva, Switzerland, 1995).

[19] S. G. Huisman, S. Scharnowski, C. Cierpka, C. J. Kähler, D. Lohse, and C. Sun, Logarithmic Boundary Layers in Strong Taylor-Couette Turbulence, Phys. Rev. Lett. **110**, 264501 (2013).

[20] R. Ostilla-Mónico, S. G. Huisman, T. J. G. Jannink, D. P. M. Van Gils, R. Verzicco, S. Grossmann, C. Sun, and D. Lohse, Optimal Taylor–Couette flow: Radius ratio dependence, J. Fluid Mech. **747**, 1 (2014).

[21] G. P. Smith and A. A. Townsend, Turbulent Couette flow between concentric cylinders at large Taylor numbers, J. Fluid Mech. **123**, 187 (1982).

[22] D. P. Lathrop, J. Fineberg, and H. L. Swinney, Transition to shear-driven turbulence in Couette-Taylor flow, Phys. Rev. A **46**, 6390 (1992).

[23] S. Huisman, R. Van Der Veen, C. Sun, and D. Lohse, Multiple states in highly turbulent Taylor–Couette flow, Nat. Commun. **5**, 3820 (2014).

[24] S. Tokgoz, G. Elsinga, R. Delfos, and J. Westerweel, Large-scale structure transitions in turbulent Taylor–Couette flow, J. Fluid Mech. **903**, A45 (2020).

[25] J. Göbel and G. Joppien, Dynamic interfacial tensions of aqueous Triton X-100 solutions in contact with air, cyclohexane, *n*-heptane, and *n*-hexadecane, J. Colloid Interface Sci. **191**, 30 (1997).

[26] S. Takagi and Y. Matsumoto, Surfactant effects on bubble motion and bubbly flows, Annu. Rev. Fluid Mech. **43**, 615 (2011).

[27] E. Llewellin, H. Mader, and S. Wilson, The rheology of a bubbly liquid, Proc. Math. Phys. Eng. Sci. **458**, 987 (2002).

[28] J. J. Stickel and R. L. Powell, Fluid mechanics and rheology of dense suspensions, Annu. Rev. Fluid Mech. **37**, 129 (2005).

[29] D. P. van Gils, D. N. Guzman, C. Sun, and D. Lohse, The importance of bubble deformability for strong drag reduction in bubbly turbulent Taylor–Couette flow, J. Fluid Mech. **722**, 317 (2013).

[30] V. Spandan, R. Verzicco, and D. Lohse, Physical mechanisms governing drag reduction in turbulent Taylor–Couette flow with finite-size deformable bubbles, J. Fluid Mech. **849**, R3 (2018).

[31] D. Lohse, Bubble puzzles: From fundamentals to applications, Phys. Rev. Fluids **3**, 110504 (2018).